Short Communication

Electrochemical Behavior of Fe-Ni Alloys as an Inert Anode for Aluminum Electrolysis

*Yipeng Huang, Youjian Yang, lingmeng Zhu, Fengguo Liu, Zhaowen Wang[*],
Bingliang Gao, Zhongning Shi, Xianwei Hu*

School of Metallurgy, Northeastern University, Shenyang 110089, China
[*]E-mail: wangzw@smm.neu.edu.cn

Fe-Ni alloys have been regarded as promising candidates for inert anodes of aluminum electrolysis. In this study, a binary Fe–Ni alloy with 32 wt% Ni content was tested as an inert anode, and its high temperature oxidation and corrosion behavior were studied. Thermogravimetric oxidation showed that the oxidation kinetics followed the parabolic law, and the oxidation rate constant was $9.568 \times 10^{-4}\,\mathrm{kg^2 \cdot m^{-4} \cdot h^{-1}}$ at 970 ℃. Fe_2O_3 and Fe-Ni-O were identified as two major components of the oxidation scale using a combination of X-ray diffraction and energy dispersive spectrometry. The anodic behavior of pre-oxidized and non-oxidized Fe–Ni alloys in cryolite-alumina melts was studied for the first time in a laboratory-scale transparent electrolysis cell. It was observed that small bubbles were released rapidly on pre-oxidized anodes, while no bubbles were generated on non-oxidized anodes and the molten electrolyte become opaque quickly. These findings confirmed that the precondition of the Fe-Ni alloy is helpful to improve its corrosion resistance.

1. INTRODUCTION

Aluminium electrolysis technology has made great advances in the past decades since its invention in 1886. However, carbon is still used as anode material in industrial electrolysis cells, which results in carbon consumption and emission of carbon dioxide and perfluorocarbon. These problems can be solved by using an inert anode (also called a non-consumable anode), and many researchers have focused on this respect. The overall reaction on inert anodes is as follows:

$$2Al_2O_3(\text{diss}) \rightarrow 3O_2 + 4Al$$
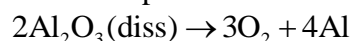
Because of the hostile operating environment and the need for good electronic conductivity, which limits many materials, most research have focused on cermet and alloy materials [1-6]. Alloys

are widely accepted for the most potential materials owing to their poor electrical resistivity and good mechanical strength. Among them, Fe-Ni alloys have received particular attention because the $NiFe_2O_4$ phase having good electrical conductivity and a low corrosion rate in cryolitic melts can be formed during electrolysis process [7-14].

For the use of alloys as inert anode materials, a protective oxide scale must be generated on the surface of the alloy during the electrolysis process to prevent the underlying metal from dissolving in the cryolitic melts. Importantly, the scale must have specific characteristics, such as low solubility in cryolitic melts and good electrical conductivity. In addition, the formed oxide scale must be self-repairing [15]. The dissolution rate of the scale should equal that of replenishment. If the replenishment rate of the scale is lower than the rate of scale dissolution, then the anode will be corroded by cryolitic melts. If the replenishment rate of the scale is higher than that of scale dissolution, a thick scale will be formed on the anode surface, resulting in a decrease in the conductivity of anode. The oxide scale is possibly generated by the following reaction during electrolysis [16]:

$$xM(s) + yO^{2-}(diss) \rightarrow M_xO_y(s) + 2ye^-$$
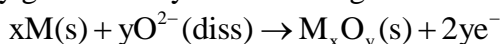
Shi et al. [17] performed oxidation tests on Fe-Ni alloy with a Ni content of 50-70 wt% at 800-900 ℃. It was found the oxidation kinetics followed the parabolic law and the components of the oxide scale were Fe_2O_3 and Fe_3O_4. Their research demonstrated the mass fraction of Ni influences the oxidation behavior of Fe-Ni alloys.

Antipov et al. [18] measured the electrochemical behavior of Ni-based anodes during galvanostatic electrolysis at 850-950 ℃. Cassayre et al. [16] studied the oxidation of Ni-Cu alloys under anodic polarization at 970 ℃. Glucina and Hyland [19] performed electrochemical tests on Al-Cu anodes for 4 h of electrolysis. In these studies, significant anode corrosion occurred because the oxide scale that formed during electrolysis was unstable.

In an attempt to decrease the anode corrosion rate in cryolitic melts during electrolysis processes, the preparation oxidation of metallic anodes was applied to improve the corrosion resistance performance. Previous studies reported the oxidation of anodes before electrolysis may contribute to improving the corrosion resistance of metallic anodes [20-22]. By appropriate selection of oxidation conditions, it is possible to form a protective scale with the desired properties. However, anode behavior under conditions of electrolysis is not well understood. In this study, the oxidation of Fe-Ni alloy in air was studied. The anodic behavior of pre-oxidized and non-oxidized Fe–Ni alloys was observed directly using transparent electrolysis cells. The corrosion behavior on the two anodes was compared and discussed in detail.

2. EXPERIMENTAL

2.1 Preparation of Fe-Ni Anodes

Fe-Ni anodes were prepared by furnace melting using Fe and Ni shot. Fe and Ni shot, which were provided by Sinopharm Chemical Reagent Co. Ltd., were reagent grade (>99%). In this study, anodes with compositions of 32 wt% Ni were prepared. The Ni and Fe shot mixed in the appropriate ratio were

melted using a medium-frequency induction furnace (ZGL-1, Xin Yan Industrial Equipment Co. Ltd., Shanghai, China) under a vacuum atmosphere. The prepared alloys were machined to 20 mm × 10 mm × 40 mm. The anode samples were polished with #5000 sandpaper and cleaned ultrasonically before use.

Table 1 shows the actual composition of the Fe-Ni alloy. These values were obtained using inductively coupled plasma-atomic emission spectroscopy (ICP-AES, Carl Zeiss AG, Germany). The intermetallic phase was studied using X-ray diffraction (XRD, PANalytical B.V., Netherlands), and the results were shown in Figure 1.

Table 1. Chemical analysis of the Fe-Ni alloy

Alloy	Fe	Ni
Theoretical composition (wt%)	68	32
Actual composition (wt%)	68.08	31.85
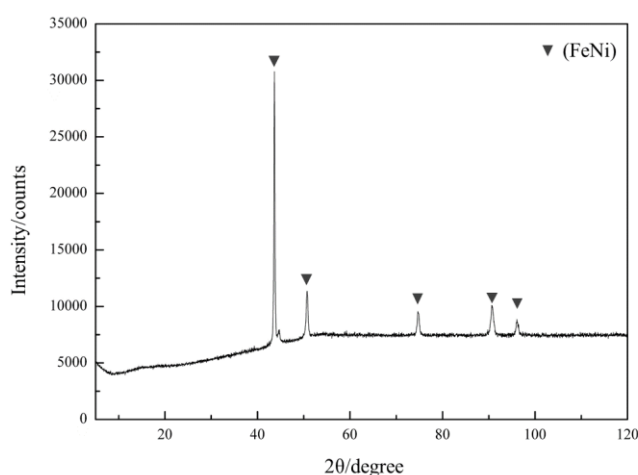
**Figure 1.** X-ray diffraction pattern of the prepared Fe-Ni alloy

2.2 Isothermal oxidation of anodes

Isothermal oxidation studies were performed in a resistance furnace under air atmosphere. The anode samples were oxidized at 970 ℃ for 22 h. A balance was used to measure the mass change of the anode samples during oxidation, and a computer connected to the balance was used to record the mass data at a frequency of 2 Hz.

2.3 Transparent aluminum electrolysis cell

A transparent aluminum electrolysis cell was used to observe the anodic behavior in molten cryolite. The experimental apparatus is shown in Figure 2. The electrolysis process was performed in a quartz crucible with two chambers (Figure 3). The two chambers were connected via a narrow gap (1 mm width) at the bottom of the separating wall. The anode and cathode were positioned in their respective

chambers. The current for electrolysis was provided by a DC power supply with a maximum voltage of 32 V (MPS702,Tradex Electronic Technology Corp, Beijing, China). A temperature controller (CKW-3100, Chaoyang Automated Instrumentation Works, Beijing, China) was used to measure and control the temperature of the furnace. The electrolysis process in the double-chamber crucible was recorded by an industrial camera (MV-VS078FC, MicroVision Company, Xi'an, China) which was positioned at the front window of the furnace. An Agilent HP34401A Digital Multi meter was used to record the cell voltage during electrolysis.
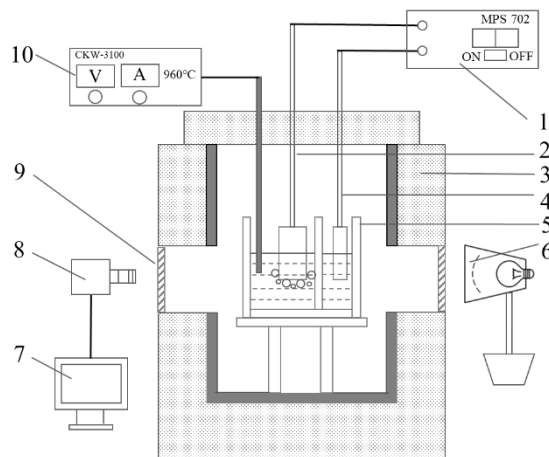
Figure 2. Schematic diagram of the transparent electrolysis cell. 1: DC power supply; 2: anode; 3: furnace; 4: cathode; 5: quartz crucible; 6: light source; 7: computer; 8: industrial cameras; 9: quartz window; 10: CKW-3100 temperature controller.

(a) Front view   (b) Top view
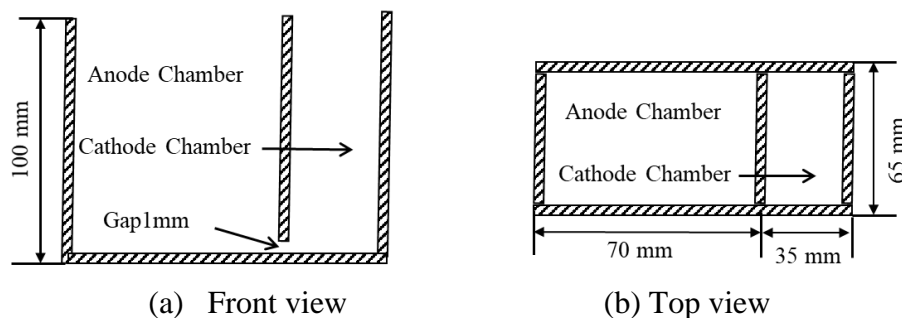
Figure 3. The double-chamber quartz crucible.

The composition of the electrolyte used in this study was 77.2 wt%Na_3AlF_6, 10.3 wt%AlF_3, 3.5 wt% Al_2O_3, 4.0 wt% CaF_2 and 5.0 wt% LiF, with a liquidus temperature of 920 ℃. All reagents were provided by Sinopharm Chemical Reagent Co. Ltd. and were high purity (>99.5%). The electrolyte mixture was dried at 673 K for 3 h before being used and stored in a dry container.

The anode sample, which was suspended into the transparent electrolysis cell above the bath to oxidize for 1h before electrolysis, was served as the pre-oxidized anode. The cathode made of graphite was shaped to the same size as the anode.

The weight of the electrolyte in each experiment was 900 g. The height of the molten bath was 70 mm. The electrolysis temperature was controlled at 942 ± 2 ℃. The immersion depth of the anode

was 25 mm. A constant current was provided during electrolysis process. The experiments were conducted at anodic current densities of 1.5 A·cm^{-2}. Short-term electrolysis was conducted for 30 min both for pre-oxidized and non-oxidized anodes. The images were recorded at 30 frames per second.

3. RESULTS AND DISCUSSION

3.1 High-temperature oxidation behavior

Figure 4 shows the evolution of specific weight gain as a function of the oxidation time at 970 ℃. Initially, the oxidation rate increased and tended to be constant for longer periods of oxidation. This indicates the thickness of the protective oxide scale increased with increasing oxidation time, which prevented the oxygen atoms from diffusing into the bulk metal. The relationship between ΔW^2 and t was close to linear by curve fitting, indicating that the oxidation kinetics followed the parabolic law, which was in agreement with previous research [17,21,23]. The oxidation rate constant was 9.568×10^{-4} kg^2·m^{-4}·h^{-1}.
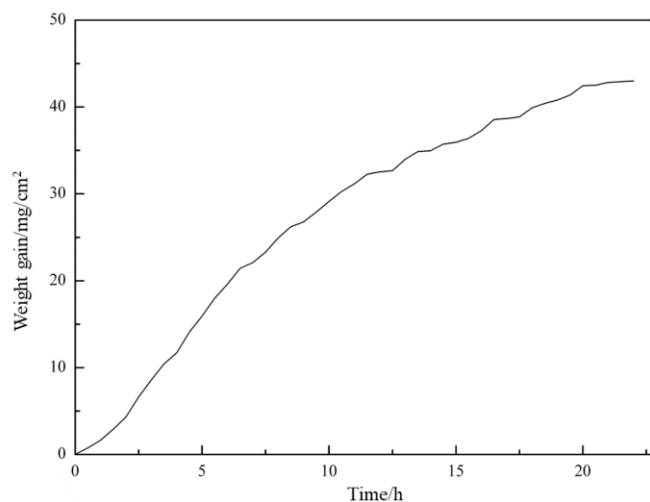

Figure 4. Weight gain variation with oxidation time for Fe-Ni alloys at 970 ℃

Figure 5 shows the XRD pattern of the surface of oxidized samples (970 ℃ for 20 h). The oxide scale was composed of Fe_2O_3 without other phase diffraction peaks. However, it is clear that the composition of the oxide scale was more complex compared to that suggested by the XRD results.
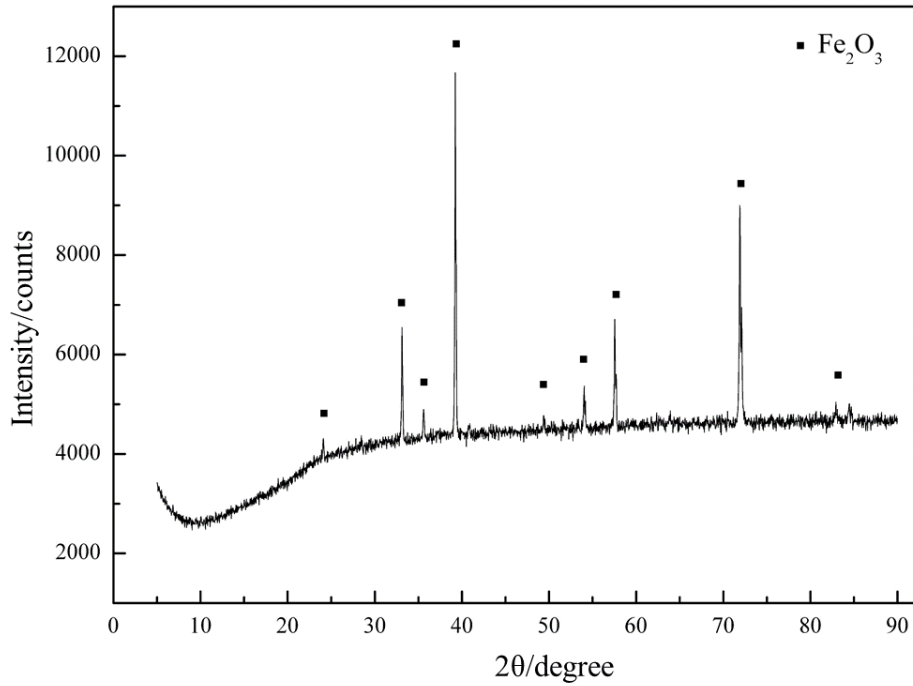
Figure 5. XRD patterns of scale on the Fe-Ni alloys after 20 h of oxidation at 970 ℃

In order to obtain more information about the compositions of the oxide scale, EDS linescans were conducted across areas of the scale. Figure 6 illustrates the element intensity plots for linescans across scale. Two different layers were observed, namely the external surface layer of Fe_2O_3 and the sequence layers of Fe-Ni-O. The underlying metal was strongly enriched with Ni. The results were confirmed by EDS surfacescans, as shown in Figure 7.
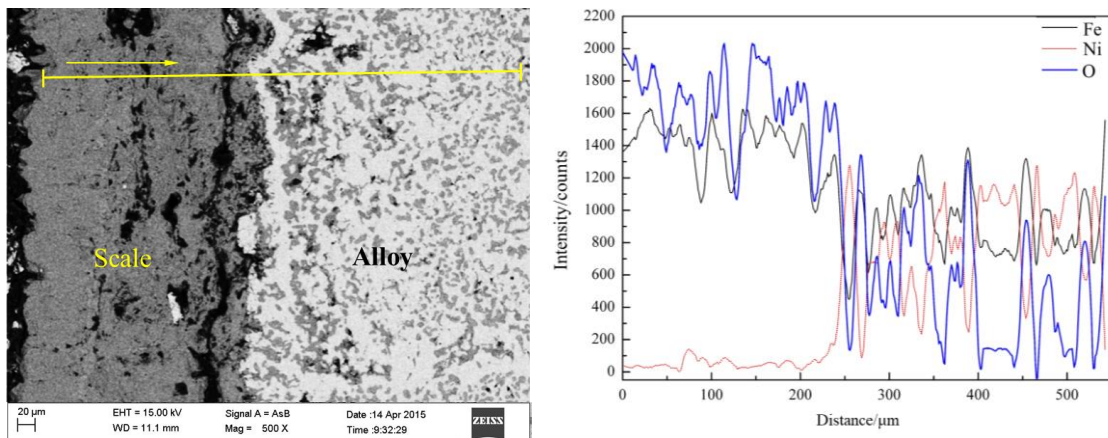
**Figure 6.** EDS linescans across scales on Fe-Ni alloys following 20 h of oxidation at 970 ℃
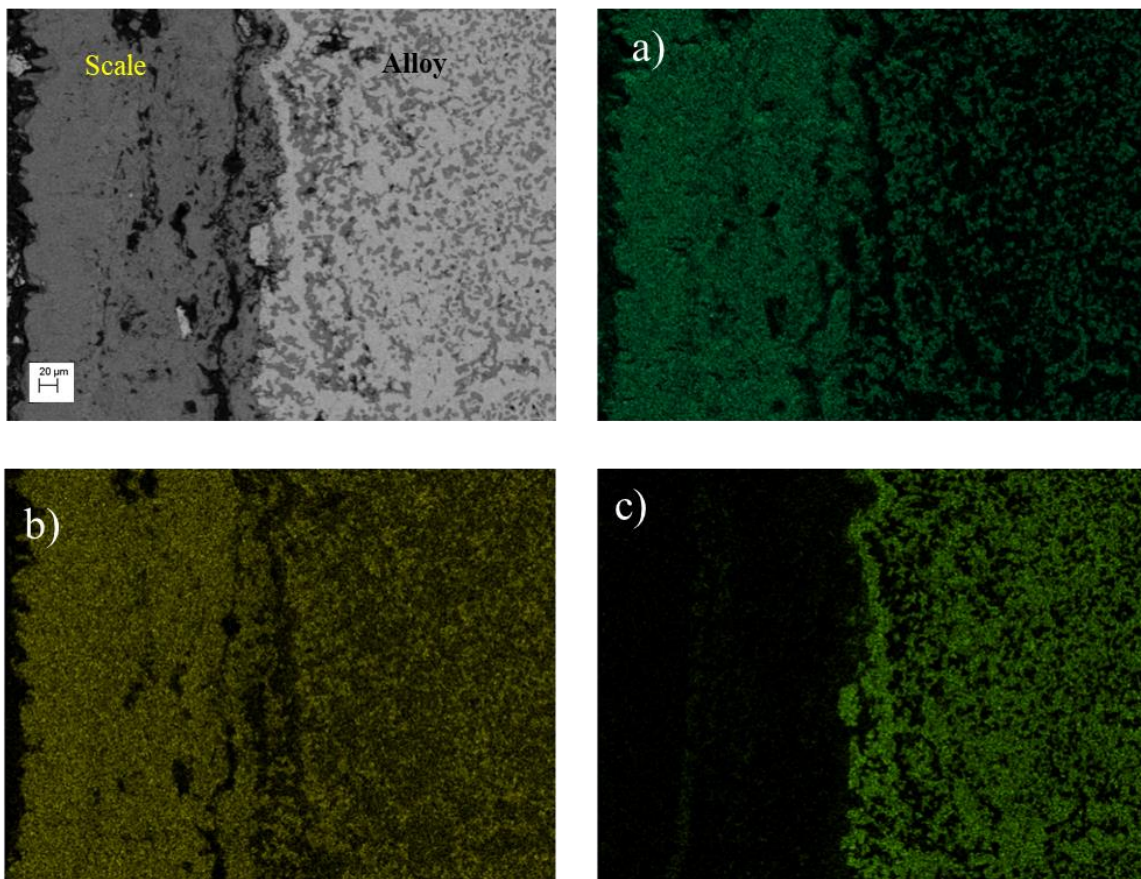
Figure 7. The surface elements distribution of oxide scale after oxidation for 20 h at 970 ℃. a) Oxygen element; b) Fe element; c) Ni element

The development of scale could be explained by the relative thermodynamic activities of Fe and Ni in the alloy. It has been confirmed that the development of scale grew with the selective oxidation of Fe to Fe_xO, where the value of x depends on the temperature and pressure of O_2 in the atmosphere [24]. When Fe from the alloy surface is oxidized, the alloy surface will become enriched with Ni. Further oxidation is limited by the diffusion of Fe from the alloy bulk to the scale interface. When the concentration of Ni at the interface reaches a critical value, formation of the $Ni_xFe_{3-x}O_4$ spinel is promoted. It is difficult for NiO to coexist with Fe_2O_3 because these two substances will react above 600 ℃ to produce the spinel phase [25].

Figure 8 shows the microphotograph of the Fe-Ni alloy at different oxidation time (1h, 10h and 20h). In all cases, many pores were formed on the oxide scale/alloy interface. Maybe it is because ferric oxides grow outward leaving vacancies in the oxide layer-alloy interface. This phenomenon is also one reason for the scale abscising from the anode surface. The results from EDS linescans analysis showed that the thickness of the scale increased with the oxidation time. At the oxidation time of 1 h, the thickness of the scale was around 64 μm. When the oxidation time increases to 20 h, the thickness of the scale was around 260 μm. This could explain the unchanged oxidation rate after longer oxidation time, as shown in Figure 4.
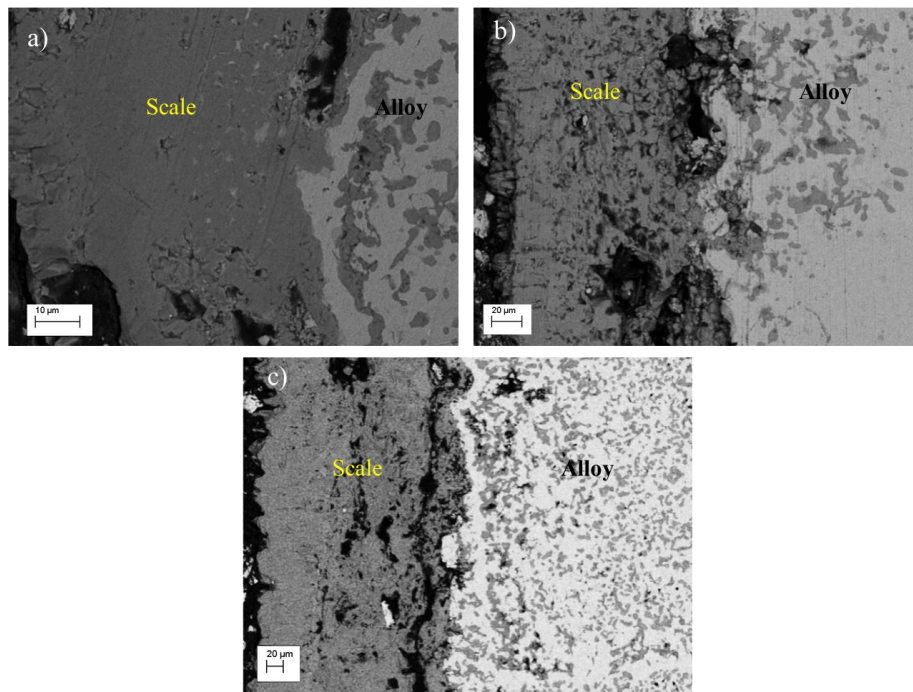
Figure 8. Scanning electron microscope images of oxide scale at 970 ℃. a) 1 h oxidation; b) 10 h oxidation; c) 20 h oxidation.

3.2 Anodic behavior in transparent electrolysis cells

Both pre-oxidized and non-oxidized anodes were subjected to constant current electrolysis in transparent electrolysis cells at 1.5 A·cm^{-2} for 30 min. Anodic behavior was observed directly from the side-view.

It is interesting to see that no bubbles were generated on the non-oxidized anode and the molten electrolyte became opaque quickly (Figure 9). Generally, the oxygen formation is expected to be the dominant anodic reaction. However, some other reactions occur under this condition. In our studies, it is difficult to determine the types of reactions that occurred at the anode. The formed oxide scale was dissolved quickly in molten salt, thus anodes underwent appreciable internal corrosion. This means stable oxide scale cannot be formed when anodes are not pre-oxidized. In our oxidation experiments, Fe_2O_3 was formed initially, however Fe_2O_3 was easily dissolved in molten electrolyte. Thus, it is difficult to form spinel which has low solubility in the bath during electrolysis.
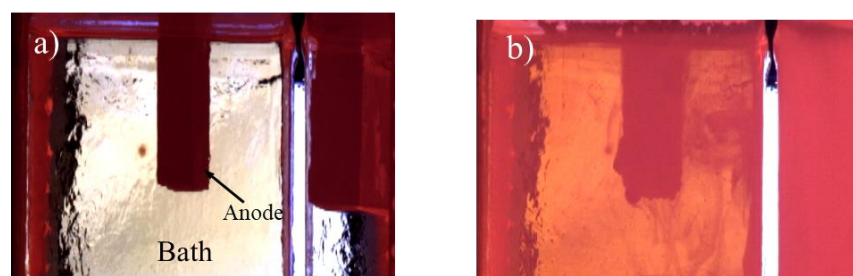

Figure 9. The electrolysis process on the non-oxidized anode at a current density of 1.5 A·cm^{-2}. a) before
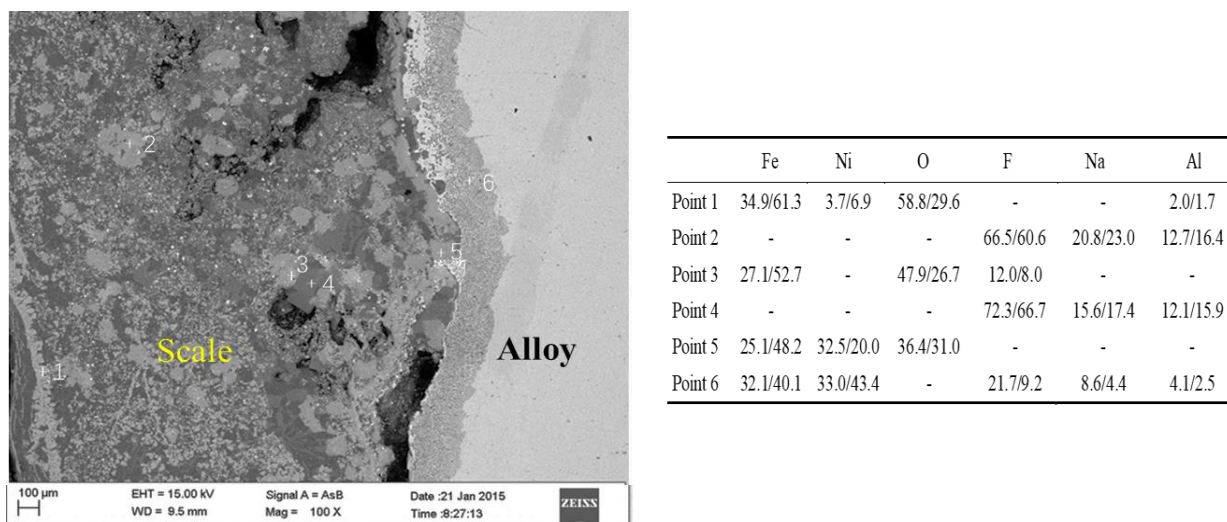
electrolysis and b) 1min after electrolysis

The rate of formation of the protective scale was lower than the dissolution rate. Therefore, anodes without per-oxidation has inferior corrosion resistance in cryolite melts. Our observations confirmed previous studies [18,19,22].

For pre-oxidized anodes, the cell voltage was relatively steady within the range of 6.8 to 7.0 V during electrolysis. Some bubbles were observed on the pre-oxidation anode during electrolysis, as shown in Figure 10. These bubbles escaped continuously without much coalescence and formed a foam around the anode, which was reported in other inert anodes [26,27]. The results demonstrated that the oxygen evolution was the primary anodic reaction on pre-oxidized anodes. In another words, the rate of formation of the protective scale is almost equal to the dissolution rate of during the electrolysis process. The results indicated the anodes that formed a protective scale before electrolysis had better corrosion resistance in cryolite melts.
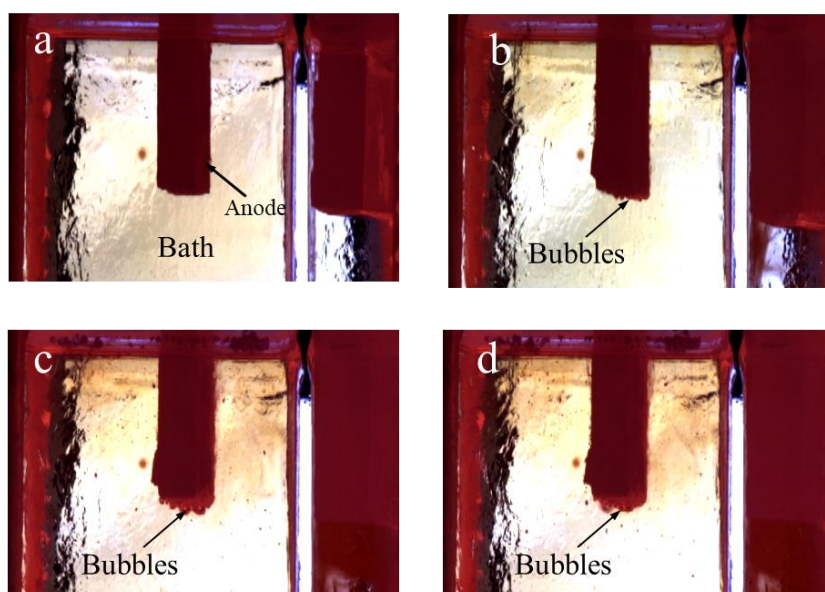
Figure 10. Bubble evolution on a pre-oxidized anode at current density of 1.5 A·cm^{-2}. a) before electrolysis; b) bubble forming; c) bubble growth; d) bubble release.

To obtain more information about the corrosion process, the pre-oxidized anode was sectioned, polished, and characterized using SEM after electrolysis experiment. The microphotograph of the pre-oxidized anode after electrolysis is shown in Figure 11. The results from EDS analysis of points 1-6 in the scale showed that the corrosion layer was divided into three layers, namely the outermost layer of Fe_2O_3, the sub-outer layer of the metal oxide mixed with electrolyte and spinel phase, and the matrix layer mixed with electrolyte. However, it is difficult to confirm if the identified scale components were produced during electrolysis or were part of the original scale formed by pre-oxidation. Meanwhile, new products were not formed during electrolysis.

	Fe	Ni	O	F	Na	Al
Point 1	34.9/61.3	3.7/6.9	58.8/29.6	-	-	2.0/1.7
Point 2	-	-	-	66.5/60.6	20.8/23.0	12.7/16.4
Point 3	27.1/52.7	-	47.9/26.7	12.0/8.0	-	-
Point 4	-	-	-	72.3/66.7	15.6/17.4	12.1/15.9
Point 5	25.1/48.2	32.5/20.0	36.4/31.0	-	-	-
Point 6	32.1/40.1	33.0/43.4	-	21.7/9.2	8.6/4.4	4.1/2.5

Figure 11. Microphotograph of Fe-Ni anodes after electrolysis experiment. The numbered markers indicate points at which quantitative analysis was performed.

Figure 10 also shows that the electrolyte penetrated to the anode interior, which caused dissolution and corrosion of the exposed metal. This phenomenon was related to the porosity of scale. The images shown in Figure 8 show that the scales generated during pre-oxidation were porous. The alloy is easily penetrated by the electrolyte when the formed scale is highly porous, resulting in internal corrosion of the metal. The porous structure of the scale is related to the composition of alloy and oxidation conditions. In addition, scale adhesion is important for effectively minimizing anode wear. It is clear that $NiFe_2O_4$ has ability to protect the anode due to its compactness and adhesiveness. Optimization of oxidation conditions, including temperature, oxidation time and oxygen concentration, may reduce the subscale corrosion.

For the pre-oxidized anodes used in this experiment, the corrosion evolution could be divided into three stages. As electrolysis occurred, the external surface layer of Fe_2O_3 began to dissolve in the molten electrolyte, and the electrolyte permeated into the inner layer through the weak part of the Fe_2O_3 scale. Then, the oxygen evolution occurred in internal scale due to spinel phase existence. At the same time, the electrolyte also penetrated into the anode interior due to the porous scale, thereby causing internal corrosion occurs. As for the continuous electrolysis the damage was continuous; internal corrosion and fluoridation occurred until the anode was completely destroyed.

4. CONCLUSIONS

Fe-Ni alloys with 32 wt% Ni were studied for application as anode material for aluminum electrolysis. Thermogravimetric oxidation studies and laboratory electrolysis tests were performed. The main conclusions are as follows:

1)   The oxidized kinetics followed parabolic rule, and the oxidation kinetics constant was $9.568 \times 10^{-4} \, kg^2 \cdot m^{-4} \cdot h^{-1}$ at 970 ℃. The oxide scale was divided into two layers: the outer layer of Fe_2O_3

and the inner layer of Fe-Ni-O. With the increasing of oxidation time, the thickness of the Fe_2O_3 layer and the Fe-Ni-O layer increases.

      2)   For the short-term electrolysis experiment, small bubbles that detached rapidly from the per-oxidized anodes were observed, while no bubbles were observed on the non-oxidized anode. Anodes without per-oxidized were shown to undergo appreciable dissolution and fluoridation. Internal corrosion also occurred in pre-oxidized anodes duo to the porous scale formed before electrolysis.

      3)   The study demonstrated that pre-oxidation of Fe-Ni alloy is very important for improving their corrosion resistance in Na_3AlF_6-Al_2O_3 melt.

References

1.   W.J Yang, L.Q. He, J. Guo, KC Zhou, *J. Adv. Microsc. Res.*, 12 (2017) 143.
2.   G.K. Ndong, J.L. Xue, L. Xing, J. Zhu, Light Metals 2015, TMS, Warrendale, USA, 2015, 83.
3.   Z.L. Tian, Y.Q. Lai, J. Li, Z.Y. Li, K.C. Zhou, and Y.X. Liu, *JOM*, 61 (2009) 34.
4.   S. Helle, M. Pedron, B. Assouli, B. Davis, D. Guay, and L. Roue, *Corros. Sci.*, 52 (2010) 3348.
5.   G.Goupil, S.Helle, B.Davis, D.Guay, L.Roué, *Electrochim Acta*, 112 (2013) 176.
6.   B. Wang, J.J. Du, Y. H. Liu, Z. Fang, P. Hu, *J. Mater. Eng. Perform.,* 26 (2017) 1.
7.   Z.L. Tian, W.C. Guo, Y.Q. Lai, K. Zhang, J. Li, *Trans. Nonferrous Met. Soc. China*, 26 (2016) 2925.
8.   D.H. Deyoung, Light Metals 2016, TMS, Warrendale, USA, 2016, 1071.
9.   Y. F. Kargin, E.N. Somoilov, V.I. Makarenkov, A.S. Lysenkov, *Inorg. Mater. Appli. Res.*, 9 (2018) 52.
10. P. Chin, P.J. Sides, R. Keller, *Can. Metall. Quart.*, 35 (1996) 61.
11. V. Chapman, B.J. Welch, M.S Kazacos, *Corros. Sci*, 53 (2011) 2815.
12. E. Olsen, J. Thonstad, *JOM*, 53 (2001) 36.
13. E. Olsen, J. Thonstad, *J. Appl. Electrochem.,* 29 (1999) 293.
14. T.E. Jentoftsen, O. A. Lorentsen, E.W. Dewing, G.M. Haarberg, J. Thonstad, *Metall. Mater. Trans. B*, 33 (2002) 901.
15. D.R. Sadoway, Light Metals 1990, TMS, Warrendale, USA, 1990, 403.
16. L. Cassayre, P. Chamelot, L. Arurault, L. Massot, P. Palau, P. Taxil, *Corros. Sci,*, 49 (2007) 3610.
17. Z.N. Shi, X.L. Zhao, J.L. Xu, Light Metals 2008, TMS, Warrendale, USA, 2008, 1051.
18. E.V. Antipov, A.G. Borzenko, V.M. Denisov, A.Y. Filatov, V.V. Ivanov, S.M. Kazakov, P.M. Mazin, V.M. Mazin, V.I. Shtanov, D.A. Simakov, G.A. Tsirlina, S.Y. Vassiliev, Y.A. Velikodny, Light Metals 2006, TMS, Warrendale, USA, 2006, 403.
19. M. Glucina, M. Hyland, *Corr. Sci.*, 48 (2006) 2457.
20. B.J. Welch, Light Metals 2009, TMS, Warrendale, USA, 2009, 971.
21. I. Gallino, M.E. Kassner, R. Busch, *Corros. Sci,*, 63 (2012) 293.
22. V. Chapman, B.J. Welch, M.S. Kazacos. *Electrochim. Acta*, 56 (2011) 1227.
23. R. Haugsrud, P. Kofstad, *Oxid. Met.*, 50 (1998) 189.
24. A. Solheim, S. Rolseth, E. Skybakmoen, L. Stoen, A. Sterten, T. Store, *Metall. Mater. Trans. B*, 27B (1996) 739.

25. R.T. Foley, *J. Electrochem. Soc,*, 109 (1962) 1202.
26. L. Cassayre, T. A. Utigard, S. Bouvet, *JOM*, 54 (2002) 41.
27. B.L. Gao, X.W. Hu, J.L. Xu, Z.N. Shi, Z.W. Wang, Z.X. Qiu. Light Metals 2006, TMS, San Antonio, USA, 2009, 467.